Deciphering the tumor-infiltrating CD73+ regulatory γδ T cell ecosystem associated with poor survival of patients with ovarian cancer

Ghita Chabab[1], Henri-Alexandre Michaud[1,2], Cécile Dejou[1], Maeva Chauvin[3], Laure-Agnès Chépeaux[1,2], Yaël Glasson[1,2], Florence Boissière[4], Marion Lenain[1], Anne-Sophie Dumé[1,2], Pauline Sarrant[1,2], Gabriel Chemin[5], Pauline Wajda[5], Bertrand Dubois[5], Anna MacManus[1,6], Pierre-Emmanuel Colombo[7], Michel Fabbro[8], Nathalie Bonnefoy[1*,] and Virginie Lafont[1*]

[1] IRCM, Institut de Recherche en Cancérologie de Montpellier, INSERM U1194, Université de Montpellier, Institut régional du Cancer de Montpellier, 34298 Montpellier, France

[2] Plateforme de Cytométrie et d'Imagerie de Masse de Montpellier, Institut de Recherche en Cancérologie de Montpellier, INSERM U1194 - UM – ICM, Montpellier, France

[3] Pediatric Surgical Research Laboratories, Massachusetts General Hospital, Boston, MA, USA - Department of Surgery, Harvard Medical School, Boston, MA, USA.

[4] Translational Research Department, Institut Régional du Cancer Montpellier, 34298 Montpellier, France

[5] Cancer Immune Surveillance and Therapeutic Targeting Laboratory, Centre de Recherche en Cancérologie de Lyon (CRCL) INSERM U1052-CNRS UMR5286, Centre Léon Bérard, Université Claude Bernard Lyon 1, France

[6] Molecular Biosciences/Cancer Biology Program, Heidelberg University and German Cancer Research Center (DKFZ), Heidelberg, Germany

[7] Oncology Surgery Department, Institut régional du Cancer de Montpellier, 34298 Montpellier, France

[8] Medical oncology Department, Institut Régional du Cancer Montpellier, 34298 Montpellier, France

[*] Co-last authors

Abstract

The ability of tumor cells to overcome immune surveillance is an essential step in tumor development and progression. Among the immune cells playing a role in tumor control, γδ T cells contribute to the immune response against many tumor types through their direct cytotoxic activity against cancer cells and their capacity to regulate the functions of other immune cells. However, their presence in the tumor microenvironment is also associated with poor prognosis, suggesting that γδ T cells may also have pro-tumor activities. We previously described a regulatory γδ T-cell subset that expresses CD73 and produces IL-10, IL-8 and adenosine. Here, we report a higher CD73+ γδ T cell density in the tumor microenvironment of ovarian cancer samples from patients with short-term than long-term survival. Starting from this original observation, we investigated their neighborhood and described a specific ecosystem according to their pro-tumor functions.

Introduction

Ovarian cancer is devastating due to its poor prognosis, with a 30% relative survival rate at 5 years, as it is usually diagnosed at an advanced stage (FIGO stage III/IV)[1]. Ovarian carcinoma accounts for over 90% of all ovarian cancer cases, and high-grade serous ovarian carcinoma (HGSOC) is the most prevalent and aggressive subtype, mainly due to resistance to platinum-based therapies[2,3]. The mechanisms underlying recurrence, metastasis and resistance to therapy in ovarian cancer may be attributed partly to the tumor microenvironment (TME), which can suppress anti-tumor immunity by recruiting and promoting immune-suppressive cells, particularly from the immune compartment[4]. In line with this, patients with HGSOC respond poorly to immune checkpoint inhibitors[5–7]. The TME can affect, positively or negatively, solid tumor progression, including ovarian cancer [8]. Indeed, the infiltration of various immune cell types into the TME is associated with the clinical outcome of patients with ovarian cancer. For example, tumor infiltration by CD3+ and CD8+ lymphocytes is associated with better survival in ovarian cancer[9,10], whereas the presence of infiltrating regulatory T cells (Tregs) predicts poor survival. Moreover, we previously showed that the

density of γδ T cells is higher in ovarian tumor tissue than in normal matched ovarian tissue and tends to be higher in FIGO III/IV (i.e. advanced cancer) than low-stage tumors[11].

γδ T cells are unconventional T lymphocytes defined by the expression of a specific T cell receptor (TCR) consisting of the Vγ and Vδ chains. In humans, there are two main γδ T-cell subtypes, depending on the Vδ chain expressed: (i) Vδ2 T cells, mainly represented by the innate Vγ9Vδ2 T-cell subset, that predominate in blood and recognize phosphorylated non-peptide antigens, called phosphoantigens; and (ii) non-Vδ2 T cells, mainly represented by the Vδ1 subset, that predominate in tissues and recognize stress-induced antigens[12–14]. Both subsets contribute to the immune response against cancer, particularly through their potent effector functions allowing direct elimination of tumor cells and the recruitment of other immune cells with anti-tumor activity[15]. However, in addition to their anti-tumor functions, γδ T cells have also been associated with pro-tumor functions in some cancer types. Specifically, IL-17A-producing γδ T cells with pro-tumoral functions have been described in murine breast, ovarian and hepatocellular cancer models and in human colorectal cancer[16–18]. In human breast cancer, γδ T cells have immunosuppressive functions associated with the induction of dendritic cell senescence[19]. Furthermore, in murine and human pancreatic ductal adenocarcinoma, γδ T cells inhibit αβ T-cell activation and their infiltration via the PD-L1/PD-1 pathway, thereby favoring tumor progression[20]. Similarly, it has been reported that in ovarian cancer, γδ T cells suppress the proliferation of CD4+ naive T cells [21]. Altogether, these data support the hypothesis that some γδ T-cell subsets may have immunosuppressive functions and favor tumor progression in some solid tumor types. In agreement, we recently identified in human blood samples a γδ T-cell subset, found in both Vδ2 and Vδ1 populations, that expresses the ectonucleotidase CD73 and produces adenosine, an immunosuppressive molecule[22,23]. This cell subset also produces IL-10 and IL-8 and inhibits conventional T-cell proliferation in a CD73/adenosine-dependent manner [22,23]. Based on these findings, here, we investigated the impact of CD73+ regulatory γδ T cells in ovarian cancer. Starting from our original observation that the presence of CD73+ γδ T cells is associated with poor clinical outcome in human ovarian cancer. We characterized the profile and investigated the neighborhood of both CD73+ and CD73- γδ T cell populations present in the ovarian TME and found a specific ecosystem according to their pro- and anti-tumor functions.

89 Materials and methods

90 ***Tissue sample collection:*** Tissue samples were from the Biological Resources Center of
91 Montpellier Cancer Institute (ICM), France, and were collected following the French
92 regulations under the supervision of an investigator. The collection was declared to the French
93 Ministry of Higher Education and Research (declaration number DC-2008–695). The study was
94 approved by the ICM Institutional Review Board (ICM-CORT-2020-32). Clinical data (e.g., age,
95 treatment, TNM, grade) were obtained by reviewing the medical files.

96 ***Ovarian cancer tumor microarray (TMA):*** TMAs regrouping 95 HGSOC samples were
97 constructed to retrospectively compare long-term (LT, >5 years) vs short-term (ST, <5 years)
98 ovarian cancer survivors. For each tumor sample, two cores (1 mm in diameter) were sampled
99 from different malignant areas. Of the 95 tumors sampled on TMA, 91 (48 LT and 43 ST) could
100 be analyzed, due to the absence of interpretable spots for 4 of them. The main
101 clinicopathological characteristics of this cohort are presented in Table S1.

102 ***Immunohistochemistry (IHC):*** 3 µm thin TMA sections were mounted on Flex microscope
103 slides (Agilent Technologies) and dried at room temperature (RT) overnight before IHC. The
104 PTLink system (Agilent Technologies) was used for de-paraffinization and heat-induced
105 antigen retrieval in High pH Buffer (Agilent Technologies) at 95°C for 15 min. IHC was
106 performed using the Dako Autostainer Link48 platform (Agilent Technologies).

107 Briefly, after endogenous peroxidase neutralization, TMA sections were incubated with the
108 mouse monoclonal anti-TCR δ antibody (Clone H-41, Santa Cruz Biotechnology) at RT for 30
109 min. This was followed by an amplification step with a mouse linker and the Flex Detection
110 System (Agilent Technologies) and 3,3'-diaminobenzidine as substrate. Sections were
111 counterstained with Flex Hematoxylin (Agilent Technologies). A NanoZoomer slide scanner
112 system (Hamamatsu Photonics) was used to digitalize the stained TMA sections with a ×40
113 objective. Immunoreactive cells were identified on the digitalized slides with the NDP.view2
114 software.

115 ***Immunofluorescence:*** After de-paraffinization, TMA sections underwent antigen retrieval
116 using 1X Target Retrieval Solution (S2367, Agilent Technologies). Then, they were incubated
117 in 1X Superblock Blocking Buffer (37515, Thermofisher) for 45 min followed by 1h incubation
118 in FcR Blocking solution (130-059-901, Miltenyi Biotech). After washing, TMA sections were

119 incubated with primary antibodies against γδ TCR (H-41, Santa Cruz, mouse, 1/25) and CD73
120 (D7AF9A, CST, rabbit, 1/100) at 4°C overnight and washed. Then, sections were incubated with
121 secondary goat anti-rabbit Alexa Fluor Plus 555 (A32732, Thermofisher) and goat anti-mouse
122 Alexa Fluor 647 (Thermofisher, A21236) antibodies. Finally, sections were counterstained with
123 DAPI and imaged with an AxioScan (Zeiss) to obtain high-power field images. TMA sections
124 were analyzed by two investigators blinded to the clinicopathological characteristics and
125 survival outcomes. Cell density was assessed by counting the number of CD73- and CD73+ γδ
126 T cells per spot (1 mm^2) and calculated as the mean of two spots.

127 ***Survival analysis***: Categorical variables were presented as frequency distributions and
128 continuous variables as medians and ranges. Categorical variables were compared with the
129 Pearson's chi-square test. Overall survival (OS) was defined as the time between the date of
130 surgery and the date of death (whatever the cause). Patients lost to follow-up were censored
131 at the last documented visit. The Kaplan–Meier method was used to estimate the OS.
132 Differences in survival rates were compared using the log–rank test. Hazard ratios (HR) are
133 given with their 95% confidence interval (95% CI). Statistical analyses were performed with
134 STATA 16.0 (StatCorp, College Station, TX, USA).

135 ***Tumor dissociation:*** Freshly samples of resected ovarian cancers HGSOC patients were cut
136 into small pieces (~1 mm^3), and incubated in RPMI medium with a digestion solution (1mg/mL
137 collagenase IV from Sigma - C5138-100mg - and 0.2 mg/mL DNase I from Roche -
138 11284932001) at 37°C for 30 min, interspaced by two rounds of mechanical dissociation with
139 gentle flushing of the mixture. The obtained single-cell suspensions were filtered and stained
140 for immunophenotyping as described in the next section.

141 ***Flow cytometry analysis:*** After dissociation, cells were washed in cold PBS and incubated with
142 a Fc receptor blocking reagent, to minimize non-specific binding of antibodies to Fc receptors,
143 and a fluorescent cell viability marker at 4°C for 15 min. Then, primary antibodies against
144 surface markers were added in PBS-2% fetal calf serum (FCS) at 4°C for 30 min. If no
145 intracellular staining was performed, cells were washed and fixed in 1% paraformaldehyde. If
146 an intracellular staining was performed, cells were washed and then fixed and permeabilized
147 using the FOXP3 Fixation and Permeabilization Kit (eBioscience) at RT for 20 min, following
148 the manufacturer's protocol. Then, cells were washed with permeabilization buffer and
149 incubated with an intracellular blocking solution (1X Permeabilization Buffer + 20% FCS) at RT

150 for 10 min. Intracellular staining was performed by incubating cells with primary conjugated
151 antibodies diluted in intracellular blocking solution at 4°C for 1 h. Cells were washed and fixed
152 in 1% paraformaldehyde. The antibodies used for flow cytometry experiments are listed in
153 Table S2. Data were acquired with a Cytoflex cytometer (Beckman-Coulter) and analyzed with
154 the FlowJo software.

155 ***Cancer-associated fibroblast (CAF) isolation from tumor samples and immunofluorescence***
156 ***staining:*** After tumor sample dissociation and filtration, the fraction left in the filters was
157 collected and cultured in DMEM-F12 with 10% FCS until full adherence. The medium was
158 changed every 2 or 3 days and cells were passaged once they reached confluence.
159 Immunofluorescence staining with antibodies against alpha smooth muscle actin (α-SMA)
160 (F3777, Sigma, 1/200) and vimentin (C9080, Sigma, 1/600) was used to confirm the CAF
161 phenotype. Cells and supernatants were then used for ELISA experiments as described below.

162 ***Ovarian cancer cell line culture:*** Cells were cultured in DMEM-F12 with 10% FCS. Medium was
163 changed every 2 or 3 days and cells were passed once they reached confluence. The
164 supernatants of confluent cells were collected for ELISA analysis.

165 ***IL-6 ELISA:*** 1.10^5 cells were plated in 48-well plates in 0.5 mL of complete cell culture medium.
166 After 24 h, cells were harvested and 0.5 mL of fresh medium was added. IL-6 production in the
167 supernatants of primary human ovarian CAF cells and four different human ovarian cancer cell
168 lines (SKOV3, OVCAR3, OVCAR8, Kuramochi) was evaluated 24 h after changing the medium
169 using the Human IL-6 DuoSet ELISA Kit (DY206-05, R&D Systems) following the manufacturer's
170 instructions.

171 ***Imaging Mass Cytometry (IMC)-based tissue selection:*** Four ovarian tumors from the ST
172 survivor group were selected based on the γδ T-cell infiltration density. From whole formalin-
173 fixed paraffin-embedded tumor blocs, three sections were cut. One was stained with
174 hematoxylin-eosin-saffron to identify tissue structures; one was used for IHC to localize γδ
175 TCR, and one for IMC labeling and analysis. Based on the IHC data, 36 regions of interest (ROI)
176 were selected and analyzed by IMC.

177 ***IMC - tissue labeling:*** After de-paraffinization and antigen retrieval using the Dako Target
178 Retrieval Solution at pH 9 (Agilent Technologies) in a water bath (96°C for 30 min), tissue
179 sections were encircled with a Dako Pen, incubated with Superblock™ (37515, Thermofisher

180 Scientific) at RT for 45 min, and then with FcR Blocking Reagent (130-092-575, Miltenyi) at RT
181 for 1 h. After three washes (8 min/each) in PBS/0.2% Triton X-100 (PBS-T), metal-tagged
182 antibodies (list in Table S3) were diluted in PBS/1% BSA buffer. After incubation with the
183 primary antibodies at 4°C overnight, sections were washed in PBS-T three times (8min/each)
184 and nuclei were stained with iridium 191 and 193 (1:400 in PBS; Standard Biotools), a DNA
185 intercalator, at RT for 30 min. Sections were washed in PBS for 5 min, then in distilled water
186 for 5 min, and dried at RT for 30 min.

187 ***IMC - data acquisition:*** Images were acquired with the Hyperion Imaging System coupled to a
188 Helios time-of-flight mass cytometer (Standard Biotools) according to the manufacturer's
189 instructions. After selection, the ROIs were ablated with a UV laser at 200Hz. The Hyperion
190 Imaging System was calibrated to ensure system stability and reproducibility following the
191 manufacturer's instructions. Data were exported as MCD files and visualized using MCD™
192 viewer 1.0.560.6.

193 ***IMC – data processing and cell segmentation***: Tiff files were extracted from the raw data,
194 denoised and segmented using a custom pipeline based on the Steinbock framework with
195 Docker container (Deepcell)[24]. Then, the segmentation masks were extracted based on the
196 iridium 191 and 193 nuclear staining and CD20, CD14, CD57, CD16, PanCK, CD3, CD66b, CD11c,
197 CD4, CD68, TCR $\gamma\delta$, CD8a, CD15, GrB, Ki67, HLA-DR and PDL1 staining (membrane/cytoplasm
198 markers). Default settings were kept for segmentation (pixel size at 1µm, whole-cell
199 segmentation, no normalization, and mean aggregation). The mean signal intensities for each
200 marker and for each cell were extracted from the .tiff files of each channel and the
201 segmentation masks with the *computeFeatures* function of the R package EBImage[25]. Then,
202 data were exported in the fcs format with the R package flowCore[26].

203 ***Manual gating:*** Hierarchically gating and specific marker intensity were used to identify
204 immune cell subsets using FlowJo v10.10 (Extended Data Fig. 2A). Positivity thresholds were
205 checked by comparing the signal intensity of a marker with its intensity on the raw image using
206 an in-house application. Then, the gates were exported and reimported into R for further
207 analysis.

208 ***Single-cell clustering :*** Immune cell clustering was performed using the Rphenograph package
209 with k=50 and based on normalized channels. Clusters with similar marker expression profiles
210 were combined with cell types to account for over-clustering.

211

212 ***IMC – Generation of neighbors:*** Neighboring cells were extracted with a homemade R
213 function. To identify its neighbors, each cell was considered as the center of a circle. Then, the
214 following formula derived from the Pythagorean theorem was used:

215 $$\sqrt{|xC - xO|^2 + |yC - yO|^2} \leq R$$

216 where *xC* and *yC* are the coordinates of the cell centroid of interest, *xO* and *yO* the coordinates
217 of other cell centroids, and R the radius defined at 12µm. For each ROI, every cell for which
218 the equation was true was considered a neighboring cell and exported in fcs format. The radius
219 distance of 12µm was chosen to identify the cells that were most likely in contact with the cell
220 of interest.

221 ***Statistical analysis:*** The Mann-Whitney, log-rank, or Wilcoxon signed rank test was used to
222 analyze the results depending on the experiment (the used tests are mentioned in the figure
223 legends). A P value <0.05 was considered significant. Analyses were performed with GraphPad
224 Prism, version 8. *p<0.05; **p<0.01; ***p<0.001; ****p<0.0001

225

226 Results

227

228 ***CD73+ γδ tumor-infiltrating lymphocytes (TILs) predict a worse clinical outcome in ovarian***
229 ***cancer***

230 We and others showed that the density of γδ T cells is higher in ovarian cancer that in normal
231 ovarian tissue samples and that the number of γδ T cells is positively correlated with advanced
232 clinicopathological features of ovarian cancer[11]. However, the impact of γδ T cells on ovarian
233 cancer outcome is still unclear. A study reported that in ovarian cancer, outcome is positively
234 influenced by the functionality of γδ T cells, measured by their ability to produce Th1
235 cytokines, and negatively affected by the proportion of CD39+ T cells[27]. Therefore, to clarify

236 their role, we analyzed the impact of γδ T-cell density on cancer progression in a cohort of 91
237 patients with ovarian cancer (n=43 ST and n=48 LT survivors) for whom clinical data were
238 collected over the years. Their median follow-up was 13.44 years (95% CI [11.67-15.47]) and
239 their median survival was 5.14 years (95% CI [3.75 - 6.08]). We first quantified by
240 immunofluorescence staining all γδ T cells and then the CD73- and CD73+ γδ T-cell subtypes.
241 The densities of total (Fig. 1A), CD73+ (Fig. 1B) and CD73- (Fig. 1C) γδ T cells were significantly
242 higher in ST survivors than in LT survivors, suggesting that the presence of γδ T cells at the
243 tumor site is associated with poor survival. We next investigated the association between
244 total, CD73+ and CD73- γδ T cells and OS in these 91 patients. OS was significantly longer in
245 patients with low density than high density of γδ T cells ($p<0.05$; Fig. 1d). Similarly, OS was
246 significantly shorter in patients with high density than low density of CD73+ γδ T cells ($p<0.001$,
247 Fig. 1E), but was not affected by the density of CD73- γδ T cells (Fig. 1F). This reinforces the
248 hypothesis that although the density of all γδ T cell subsets is higher in ST survivors, the effect
249 γδ T cells on survival is mostly due to the CD73+ subset. This suggests that the presence and
250 density of CD73+ γδ T cells is a potential prognostic marker in ovarian cancer.

251 In parallel, the analysis of TCGA data revealed a strong association between a CD73+ tumor
252 microenvironment and poor patient outcomes (Fig. 2A). To investigate whether this CD73+
253 microenvironment correlates with γδ T cell infiltration, contributing to reduce survival as
254 demonstrated in Figure 1, we analyzed single-cell RNA sequencing (scRNA-seq) data from 20
255 treatment-naive ovarian cancer samples. These samples were pooled and extracted from the
256 GSE147082, GSE241221, and GSE235931 datasets [28,29] (Fig. 2B). Patients were divided into two
257 groups based on median NT5E/CD73 expression levels: NT5E-Low and NT5E-High (N=10 per
258 group) (Fig. 2B). Interestingly, expressions of specific γδ T cell transcripts such as *TRDC, TRGC1,*
259 *TRGC2 are higher in TME overexpressing NT5E. In addition, the following cytokine expression*
260 *CXCL8, IL-10, IL-6* (Fig. 2C and 2D), associated with higher proportion of CAFs (Fig. 2E) was
261 higher in the CD73/NT5E-High than CD73/NT5E-Low group. This population enrichment
262 suggests that the expression of IL-6, IL-10 and CXCL8 and the density of γδ T cells and CAFs are
263 higher in CD73/NT5E-rich TMEs than in CD73/NT5E-low TMEs. To validate these observations
264 and to further explore these relationships between cell subsets in different TMEs, we
265 performed a spatial proteomic analysis using an innovative high-plexed technology to describe
266 each cell phenotype and ecosystem.

267 ***Cell composition of human ovarian tumors from short-term survivors***

268 First, we investigated the tissue composition of four ovarian tumor samples from the ST
269 survivor group of our cohort by multiplexed IMC using a specific protocol described in
270 Extended Data Fig. 1. We selected 36 ROIs corresponding to approximately 56 mm^2 based on
271 the γδ T-cell density identified by IHC, on a serial section. Using a 31-marker panel (Table S3)
272 and a specific gating strategy to identify tumor, stromal and immune cells (Extended Data Fig.
273 2A-B), we analyzed the cell composition of the selected ROIs (Extended Data Fig. 2C-D). We
274 identified 17 cell types and observed heterogeneity among tumor samples and ROIs. Tumor
275 cells, identified as E-cadherin+ and PanCK+ cells, were the most important cell type in all
276 samples (46% of all cells), followed by immune cells (27% of all cells) and fibroblasts (vimentin+
277 cells; 15% of all cells) (Extended Data Fig. 2E). Moreover, α-SMA+ cells were 8% of all cells and
278 <1% of cells represented the vascular compartment (Extended Data Fig. 2E-F). The remaining
279 cells (<3.5%), classified as "undetermined" (Extended Data Fig. 2C-E), corresponded to cells
280 with a nucleus, but that could not be identified using our panel. The characterization of the
281 immune infiltrate (Extended Data Fig. 2d and f) showed that lymphoid cells represented ~75%
282 of the immune infiltrate and most of them were T cells. In the myeloid compartment,
283 monocyte-derived dendritic cells were the most abundant subset (~13%).

284

285 ***Phenotypic analysis of CD73+ and CD73- γδ TILs***

286 Based on γδ TCR expression, we analyzed the γδ T-cell compartments by IMC (Fig. 3A). The
287 proportion of γδ T cells was quite homogenous in all ROIs. They represented ~3% of the
288 immune compartment (Fig. C and ~20% of all γδ TILs were CD73+ (Fig. 3D). Although the ROIs
289 analyzed by IMC were selected based on the presence of γδ T cells, the results were consistent
290 with the flow cytometry (FC) data obtained using fresh ovarian tumor samples (n=7) (Fig. 3B-
291 D).

292 Unsupervised analysis of total γδ T cells from the IMC data allowed identifying eight clusters
293 based on the expression of immune checkpoints and functional markers (Fig. 3E). The tSNE
294 plots of the CD73+ and CD73- γδ T-cell subsets were clearly different (Fig. 3F). Clusters 1, 5, 6
295 and 8 were more abundant in the CD73- γδ T-cell subset, whereas clusters 3 and 7 were more
296 abundant in the CD73+ γδ T-cell subset (Fig. 3F and Extended Data Fig. 3A). Cluster 3 was

297 characterized by strong expression of PD-L1 and to a lesser extent of LAG-3 and TIM-3 (Fig. 3E
298 and G) and cluster 7 by expression of PD-1, LAG-3, CD39 and Ki-67. Among the most abundant
299 clusters in the CD73- γδ T-cell subset, cluster 1 was characterized by high expression of the
300 functional marker HLA-DR and the immune checkpoints TIM-3, PD-L1 and LAG-3; cluster 5 by
301 expression of the immune checkpoints PD-1, CD39, LAG-3, Ki-67, and cluster 6 by expression
302 of HLA-DR and PD-L1. Cluster 8 was not characterized by any of the analyzed markers (Fig. 3E-
303 G). Clusters 2 and 4 were not specific to any subset. In parallel, we performed conventional
304 flow cytometry analysis of immune checkpoint marker expression in fresh ovarian tumor
305 samples (n=7). We confirmed the higher expression of PD-L1 in the CD73+ γδ T-cell subset.
306 PD-L2 also was expressed in this subset, whereas TIGIT was more strongly expressed in the
307 CD73- γδ T-cell subset (Extended Data Fig. 3B). This suggested that PD-L1 or PD-L2 expression
308 also may contribute to the immunosuppressive functions of CD73+ γδ T cells.

309 We previously showed that regulatory γδ T-cell subsets, derived from *in vitro* culture of blood
310 healthy donors, are characterized by CD73 expression and IL-8 and IL-10 production.
311 Therefore, we investigated by flow cytometry the expression IFN-γ, IL-10 and IL-8 by γδ T cells
312 isolated from fresh ovarian cancer samples in correlation with CD73 expression (Fig. 3H). The
313 frequency of IL-8+ and IL-10+ cells was significantly higher in the CD73+ γδ than in the CD73-
314 γδ T-cell subset (75% versus 10% for IL-8, 45% versus 5% for IL-10). Moreover, 35% of CD73+
315 γδ T cells expressed both cytokines. Conversely, the percentage of IFN-γ+ cells was
316 significantly higher in the CD73- than CD73+ γδ T-cell subset (70% versus 30%). Altogether,
317 these results demonstrated that CD73+ γδ T cells from ovarian tumors have a profile similar
318 to that of the previously described regulatory CD73+ γδ T-cell subset[22,23] and suggested that
319 their immunosuppressive properties may be involved in the poorer clinical outcome.

320

321 ***CD73+ and CD73- γδ TILs have phenotypically and functionally different ecosystems***

322 Besides the immune cell composition, the spatial location and interactions of immune cells
323 within the TME are essential for their functions and the effect on tumor development and
324 response to treatment.
325 Here, we investigated the γδ T-cell ecosystem by comparing the effector (CD73-) and
326 regulatory (CD73+) γδ T-cell neighborhoods and interactions by IMC. After identification and

327 localization of CD73+ and CD73- γδ T cells in ovarian cancer tissue sections (Fig. 4A), we
328 measured and compared the individual interactions between CD73+ and CD73- γδ T cells with
329 the other identified cell types. For both cell subtypes, we observed a heterogenous
330 environment but with significant differences. CD73- γδ T cells had a neighborhood significantly
331 enriched in tumor cells (24.4% versus 12.7% for CD73+ γδ T cells) (Fig. 4B and Extended Data
332 Fig. 4). Conversely, fibroblasts and CD4+ T cells tended to be more frequently in contact with
333 CD73+ than CD73- γδ T cells (Fig. 4B and c and Extended Data Fig. 4), suggesting that the CD73+
334 γδ T-cell neighborhood is enriched in fibroblasts and CD4+ T cells. Comparison of the CD73+
335 γδ T-cell ecosystem with the conventional regulatory T-cell (CD3+CD4+FOXP3+) ecosystem
336 revealed a specific CD73+ γδ T cell ecosystem (Extended Data Fig. 5).

337 We then determined the number of cells for all identified populations and chose to perform
338 a functional analysis only of the cell compartments containing more than 750 cells to obtain
339 robust results (Extended Data Fig. 6): tumor cells, fibroblasts, CD4+ and CD8+ T cells.

340 Unsupervised clustering of the tumor cell compartment allowed identifying eight cell
341 populations that were differentially abundant depending on whether they were in the vicinity
342 of effector or regulator γδ T cells (Fig. 5A and Extended Data Fig. 7A Indeed, tumor cells in the
343 neighborhood of CD73+ γδ T cells expressed CD73 and the epithelial-to-mesenchymal
344 transition (EMT) marker ZEB-1, suggesting migratory capacity (Fig. 5A). Tumor cells in contact
345 with CD73- γδ T cells expressed PD-L1. Altogether, these data suggest that tumor cells in
346 contact with CD73+ γδ T cells have a more aggressive phenotype. Similarly, cluster analysis
347 showed that fibroblasts in contact with CD73+ γδ T cells expressed CD73 and PD-L1, whereas
348 those in contact with CD73- γδ T cells expressed more CD39 and Ki-67 (Fig. 5B and Extended
349 Data Fig 7B).

350 Like for other cell types, unsupervised analysis of the T-cell compartment gave different tSNE
351 clustering plots in the neighborhood of CD73+ and CD73- γδ T cells for the CD4+ and CD8+ T
352 cell populations (Fig. 6A-B and Extended Data Fig. 7C-D). The cluster analysis revealed that
353 CD4+ T cells in contact with effector γδ T cells (i.e. the CD73- subset) had an activated state
354 with expression of HLA-DR and/or PD-1. Conversely, those in contact with CD73+ γδ T cells
355 expressed CD73, PD-1, CD39 and LAG-3, suggesting an exhausted phenotype (Fig. 6A). For
356 CD8+ T cells, the CD73+ and PD-1+ cluster was much more abundant in the neighborhood of
357 CD73+ γδ T cells (Extended Data Fig 7D).

358 Although the density of fibroblasts and T cells surrounding CD73- and CD73+ γδ T cells was
359 similar, the functional phenotype of these cell populations was different, resulting in distinct
360 ecosystems, suggesting that CD73+ γδ T cells are located in an immunosuppressive niche in
361 close contact with tumor cells. Comparison of CD73+ γδ T cells and Treg revealed specific
362 neighborhoods for each population (Extended Data Fig. 5), suggesting that the mechanisms
363 responsible for establishing an immunosuppressive microenvironment are specific to CD73+
364 regulatory γδ T cells.

365 ***Impact of IL-6 produced by ovarian CAFs and tumor cells on γδ T cells***

366 We and others provided evidence that soluble factors, such as cytokines, can modulate the
367 functions of γδ T cells[30]. Specifically, we showed that IL-21 promotes the development of a
368 pro-tumoral γδ T-cell subset, characterized by CD73 expression and production of
369 immunosuppressive molecules, such as adenosine, IL-10 and IL-8[22] . Others have shown that
370 CAFs from breast tumors produce IL-6 and induce the differentiation of CD73+ γδ T cells from
371 normal breast tissue into immunosuppressive T cells[31]. As IL-6 is strongly expressed in the
372 ovarian TME [32], we hypothesized that CAF-produced IL-6 may be involved in the development
373 of CD73+ γδ T cells in ovarian cancer. We isolated CAFs from freshly resected ovarian tumor
374 samples (n=3) and confirmed their phenotype/purity by α-SMA and vimentin staining
375 (Extended Data Fig. 9A). We then measured IL-6 in their supernatants and in the supernatants
376 of four ovarian tumor cell lines by ELISA. Both CAFs and ovarian tumor cell lines produced IL-
377 6, but the amounts were much higher in CAF supernatants than in tumor cells (1500 pg/mL vs
378 ~70pg/mL) (Extended Data Fig. 9B). Moreover, tumoroids generated from freshly resected
379 human ovarian tumors produced IL-6 (data not shown). In addition, we confirmed that IL-6,
380 like IL-21, promoted the development of the CD73+ γδ T cell subset from blood γδ T cells of
381 healthy donors (Extended Data Fig. 9C). Altogether, these data suggest that the cross-talk
382 between CAFs and γδ T cells in the TME through Il-6 production may favor an
383 immunosuppressive niche that promotes tumor growth and immune escape.
384

385 Discussion

386 Investigating the presence, functions and location of immune cells in the TME is essential for
387 developing effective immunotherapy strategies. In this study, we report the presence of
388 CD73+ γδ T cells, a regulatory γδ T-cell subset with immunosuppressive functions, in the
389 ovarian TME and show that their density is associated with poorer clinical outcome in these
390 patients. Although γδ T cells have often been associated with good cancer prognosis[33], several
391 reports in ovarian cancer have provided evidence of their negative impact. For instance, γδ T
392 cells have been positively associated with advanced clinicopathological features of ovarian
393 cancer [34]. Moreover, the presence of Vδ1+ cells correlates with progression-free and OS in
394 patients with triple-negative breast cancer[35]. Conversely, CD73+ γδ T cell infiltration has been
395 correlated with worse clinical outcome in patients with breast cancer [31]. In line with our
396 findings in ovarian cancer, the CD73+ γδ T-cell subset appears to be involved in poor outcome
397 in some cancer types, but the involved mechanisms remain to be elucidated.

398 By combining scRNA-seq, high-plex IMC and *ex vivo* flow cytometry analysis of freshly resected ovarian
399 tumors, we described in detail the phenotype and ecosystem of CD73+ and CD73- γδ T cells.
400 CD73+ γδ T cells produce IL-10 and IL-8 and also express the immune checkpoints PD-L1 and
401 PD-L2, cytokines and ligands that may explain their regulatory functions and may be involved
402 in the immunosuppressive or pro-tumor mechanisms leading to tumor progression. Indeed,
403 IL-10 impairs the functions of effector cells, such as T and natural killer cells, while PD-L1 and
404 PD-L2 contribute to tumor immune evasion by binding to PD-1 and impair the function of all
405 PD-1+ effector immune cells. IL-8, also known as CXCL8, was originally classified as a
406 chemoattractant for neutrophils and myeloid-derived suppressor cells. It is now known to play
407 other important biological activities in various solid cancer types, such as induction/regulation
408 of angiogenesis and promotion of cancer cell growth, survival and migration[36,37]. Several
409 studies have shown that IL-8 induces EMT in ovarian cancer cells and favors migration,
410 invasion and metastasis formation[38–40]. IL-8 also promotes ovarian cancer growth in 3D
411 spheroid models [41]. Moreover, CAF-derived IL-8 promotes the stemness and malignant
412 proliferation of ovarian cancer cells through NOTCH-3 signaling pathways[42]. Conversely, CD73-
413 γδ T cells produce IFN-γ, express the PD-1 and TIGIT checkpoint molecules, and also HLA-DR.
414 Several studies have shown that human γδ T cells can express MHC class II molecules and
415 acquire professional antigen-presenting cell characteristics. Thus, ovarian CD73- γδ TILS have
416 effector T cell properties, whereas CD73+ γδ TILS have regulatory T cell properties.

417 We also performed a spatial analysis of the CD73+ and CD73- γδ T cell ecosystems in ovarian
418 cancer samples. We found that CD73+ γδ T cells were in close contact with more aggressive
419 tumor cells, particularly those expressing ZEB-1, a transcription factor associated with EMT.
420 This is consistent with CD73+ γδ T cell ability to produce IL-8, which has been described as an
421 inducer of several transcription factors involved in EMT and tumor cell migration, such as ZEB-
422 1 and snail[43]. In addition, tumor cells close to CD73+ γδ T cells also expressed CD73, which is
423 involved in the generation of the immunosuppressive molecule adenosine from AMP present
424 in the TME. Conversely, tumor cells adjacent to CD73- γδ TILs expressed the immune
425 checkpoint PD-L1 that can be induced by IFN-γ, a cytokine largely produced by CD73- γδ T cells
426 ([44] and our experiments). The spatial analysis also revealed that fibroblasts/CAFs in contact
427 with CD73+ γδ T cells are functionally distinct from those in contact with the CD73- subset.
428 Specifically, one of the CAF clusters in contact with the CD73+ γδ T-cell subset expressed CD73.
429 Several studies have described CD73+ CAF subsets as tumor-promoting or
430 immunosuppressive CAFs. Using a 41-plex antibody panel designed to discriminate the
431 different CAF phenotypes by mass cytometry, Bodenmiller's group identified a subset, which
432 they termed tumor-like CAFs (tCAFs), with tumor-promoting and immunosuppressive effects
433 and characterized by CD73 and CD10 expression[45]. Another study using a mouse model of soft
434 tissue sarcoma identified a CAF subset with a glycolytic signature and characterized by CD73
435 expression. These glycolytic CAFs rely on GLUT-1-dependent expression of CXCL16 to prevent
436 cytotoxic T-cell infiltration into the tumor. Therefore, CD73+ CAFs could be considered as
437 immunosuppressive or pro-tumor CAFs. In the T-cell compartment, the spatial analysis
438 revealed a cluster of CD4+ T cells with an activated profile that expressed HLA-DR and/or PD-
439 1 in the neighborhood of the CD73- γδ T-cell subset. Conversely, those in contact with CD73+
440 γδ T cells expressed CD73, PD-1, CD39 and LAG-3, suggesting an exhausted phenotype. The
441 spatial analysis of CD8+ T cells highlighted a different clustering between cells in contact with
442 CD73- and CD73+ γδ T cells, particularly concerning the expression of immune checkpoint
443 factors. Indeed, those in contact with CD73+ γδ T cells expressed PD-1 and CD39, whereas
444 those contact with CD73+ γδ T cells expressed CD73 and Lag-3.
445 Cytokines can promote or inhibit tumor cell differentiation and immune cell
446 differentiation/functions and angiogenesis, and ultimately affect the patients' response to
447 therapy[25]. Ovarian tumors are characterized by abnormal expression of many cytokines, such
448 as IL-6, IL-8 and IL-10, that affects all TME components and also patient survival[26,27]. IL-8 and

449 IL-10 are produced by CD73+ γδ T cells and IL-6 by cells in their close environment. Other
450 cytokines that can have an immunosuppressive effect, such as IL-17A and TGF-β, can be
451 produced by some γδ T-cell subsets and be involved in the immunosuppressive mechanisms
452 of γδ T cells and/or in their effect on tumor growth, as demonstrated in human colorectal
453 cancer where IL-17A is produced by γδ T cells [18]. However, in the present study, ovarian cancer
454 CD73+ γδ T cell subsets did not produce these two cytokines (data not shown).

455 Studies in other cancer types demonstrated the existence of immunosuppressive or pro-
456 tumor γδ T-cell subsets. Daley et al showed in a murine pancreatic cancer model that tumor-
457 infiltrating γδ T cells have potent immunosuppressive functions through the PD-1/PD-L1 axis[20].
458 Specifically, 50% of infiltrating γδ T cells express PD-L1 and induce αβ T-cell exhaustion
459 through this mechanism. In our study, regulatory γδ T cells were characterized by the
460 expression of CD73 and of various immune checkpoint factors, such as PD-L1. This suggests
461 that in addition to the effects mediated by IL-10 and IL-8, CD73+ γδ T cells may mediate
462 immunosuppression and promote cancer growth through immune checkpoint factor
463 expression and adenosine production. In colorectal cancer, Lynch's group described a γδ T-
464 cell subset that expresses NKp80, produces AREG and induces tumor cell proliferation[46]. The
465 existence of pro-tumor and immunosuppressive γδ T-cell subsets is now well established and
466 their role in some cancer types has been demonstrated; however, they represent a
467 heterogeneous population with different mechanisms.

468 Chronic inflammation is a cancer hallmark and is involved in tumor development and
469 progression. Inflammatory cytokines mediate chronic inflammation and are involved in cancer
470 progression by regulating, for example, immune cell functions. IL-6, which is present at high
471 levels in the ovarian TME, is associated with poor prognosis and increased tumor
472 progression[39,40]. We and others reported that in ovarian tumors, IL-6 is mainly produced by
473 CAFs and induces CD73 expression by γδ T cells (Extended Data Fig. 9 and [15]). Thus, the
474 proximity between CD73+ γδ T cells and CAFs, observed by IMC, suggests crosstalk
475 mechanisms whereby CAF-produced IL-6 would lead to the recruitment or polarization of γδ
476 T cells into regulatory CD73+ γδ T cells. By a positive feedback, adenosine produced by CD73+
477 cells would increase IL-6 production in the ovarian TME (Fig. 7). These findings are consistent
478 with the work by Hu et al, who showed that in human breast cancer, CAF-derived IL-6 induces
479 γδ T-cell differentiation into the regulatory CD73+ subset which produces high levels of

480 adenosine following the activation of the IL-6/IL6-R/STAT3 signaling pathway[31]. They also
481 showed that CD73+ γδ T cells could in turn promote IL-6 secretion by CAFs through activation
482 of the adenosine/A2BR/p38 MAPK pathway, thereby forming a positive feedback loop[31]. This
483 interplay between CAFs and CD73+ γδ T cells could be a general mechanism in solid tumors.
484 The role of IL-8 in EMT and tumor cell migration cells could also be included in this regulation
485 loop, as shown in Figure 7. Our preliminary data show that CD73+ γδ T cells are present in
486 pancreatic and colorectal cancer (data not shown), but their ecosystem remains to be
487 investigated. Overall, our data provide a better understanding of the role of regulatory γδ T
488 cells in the tumor microenvironment and allow to propose mechanisms involving γδ T cells in
489 the creation of a specific immunosuppressive environment (Fig. 7), which could be a more
490 general and existing mechanism in solid tumors with a poor evolution.

491

492

493 References

494 1. Sung, H. *et al.* Global Cancer Statistics 2020: GLOBOCAN Estimates of Incidence and
495 Mortality Worldwide for 36 Cancers in 185 Countries. *CA: A Cancer Journal for Clinicians*
496 **71**, 209–249 (2021).

497 2. Hinchcliff, E., Westin, S. N. & Herzog, T. J. State of the science: Contemporary front-line
498 treatment of advanced ovarian cancer. *Gynecologic Oncology* **166**, 18–24 (2022).

499 3. Luvero, D., Milani, A. & Ledermann, J. A. Treatment options in recurrent ovarian cancer:
500 latest evidence and clinical potential. *Ther Adv Med Oncol* **6**, 229–239 (2014).

501 4. Drakes, M. L. & Stiff, P. J. Regulation of Ovarian Cancer Prognosis by Immune Cells in the
502 Tumor Microenvironment. *Cancers (Basel)* **10**, 302 (2018).

503 5. Hamanishi, J. *et al.* Programmed cell death 1 ligand 1 and tumor-infiltrating CD8+ T
504 lymphocytes are prognostic factors of human ovarian cancer. *Proc Natl Acad Sci U S A* **104**,
505 3360–3365 (2007).

506 6. Disis, M. L. *et al.* Efficacy and Safety of Avelumab for Patients With Recurrent or Refractory
507 Ovarian Cancer: Phase 1b Results From the JAVELIN Solid Tumor Trial. *JAMA Oncol* **5**, 393–
508 401 (2019).
509 7. Ray-Coquard, I. L. *et al.* Neoadjuvant and adjuvant pembrolizumab in advanced high-grade
510 serous carcinoma: the randomized phase II NeoPembrOV clinical trial. *Nat Commun* **15**,
511 5931 (2024).
512 8. Baci, D. *et al.* The Ovarian Cancer Tumor Immune Microenvironment (TIME) as Target for
513 Therapy: A Focus on Innate Immunity Cells as Therapeutic Effectors. *Int J Mol Sci* **21**, 3125
514 (2020).
515 9. Ovarian Tumor Tissue Analysis (OTTA) Consortium *et al.* Dose-Response Association of
516 CD8+ Tumor-Infiltrating Lymphocytes and Survival Time in High-Grade Serous Ovarian
517 Cancer. *JAMA Oncol* **3**, e173290 (2017).
518 10. Zhang, L. *et al.* Intratumoral T cells, recurrence, and survival in epithelial ovarian cancer.
519 *N Engl J Med* **348**, 203–213 (2003).
520 11. Chabab, G. *et al.* Diversity of Tumor-Infiltrating, γδ T-Cell Abundance in Solid Cancers. *Cells*
521 **9**, 1537 (2020).
522 12. Kabelitz, D. γδ T-cells: cross-talk between innate and adaptive immunity. *Cell Mol Life Sci*
523 **68**, 2331–2333 (2011).
524 13. Vantourout, P. & Hayday, A. Six-of-the-best: unique contributions of γδ T cells to
525 immunology. *Nat Rev Immunol* **13**, 88–100 (2013).
526 14. Adams, E. J., Gu, S. & Luoma, A. M. Human gamma delta T cells: Evolution and ligand
527 recognition. *Cell Immunol* **296**, 31–40 (2015).
528 15. Kabelitz, D., Serrano, R., Kouakanou, L., Peters, C. & Kalyan, S. Cancer immunotherapy with
529 γδ T cells: many paths ahead of us. *Cell Mol Immunol* **17**, 925–939 (2020).

530 16. Coffelt, S. B. *et al.* IL-17-producing γδ T cells and neutrophils conspire to promote breast
531 cancer metastasis. *Nature* **522**, 345–348 (2015).
532 17. Ma, S. *et al.* IL-17A produced by γδ T cells promotes tumor growth in hepatocellular
533 carcinoma. *Cancer Res* **74**, 1969–1982 (2014).
534 18. Wu, P. *et al.* γδT17 cells promote the accumulation and expansion of myeloid-derived
535 suppressor cells in human colorectal cancer. *Immunity* **40**, 785–800 (2014).
536 19. Peng, G. *et al.* Tumor-infiltrating gammadelta T cells suppress T and dendritic cell function
537 via mechanisms controlled by a unique toll-like receptor signaling pathway. *Immunity* **27**,
538 334–348 (2007).
539 20. Daley, D. *et al.* γδ T Cells Support Pancreatic Oncogenesis by Restraining αβ T Cell
540 Activation. *Cell* **166**, 1485-1499.e15 (2016).
541 21. Chen, X. *et al.* Distribution and functions of γδ T cells infiltrated in the ovarian cancer
542 microenvironment. *J Transl Med* **17**, 144 (2019).
543 22. Barjon, C. *et al.* IL-21 promotes the development of a CD73-positive Vγ9Vδ2 T cell
544 regulatory population. *Oncoimmunology* **7**, e1379642 (2017).
545 23. Chabab, G. *et al.* Identification of a regulatory Vδ1 gamma delta T cell subpopulation
546 expressing CD73 in human breast cancer. *J Leukoc Biol* **107**, 1057–1067 (2020).
547 24. Windhager, J. *et al.* An end-to-end workflow for multiplexed image processing and
548 analysis. *Nat Protoc* **18**, 3565–3613 (2023).
549 25. Pau, G., Fuchs, F., Sklyar, O., Boutros, M. & Huber, W. EBImage--an R package for image
550 processing with applications to cellular phenotypes. *Bioinformatics* **26**, 979–981 (2010).
551 26. Hahne, F. *et al.* flowCore: a Bioconductor package for high throughput flow cytometry.
552 *BMC Bioinformatics* **10**, 106 (2009).

553 27. Foord, E., Arruda, L. C. M., Gaballa, A., Klynning, C. & Uhlin, M. Characterization of ascites-
554 and tumor-infiltrating γδ T cells reveals distinct repertoires and a beneficial role in ovarian
555 cancer. *Sci Transl Med* **13**, eabb0192 (2021).
556 28. Kang, H. *et al.* Altered tumor signature and T-cell profile after chemotherapy reveal new
557 therapeutic opportunities in high-grade serous ovarian carcinoma. *Cancer Sci* **115**, 989–
558 1000 (2024).
559 29. Olalekan, S., Xie, B., Back, R., Eckart, H. & Basu, A. Characterizing the tumor
560 microenvironment of metastatic ovarian cancer by single-cell transcriptomics. *Cell Rep* **35**,
561 109165 (2021).
562 30. Zhao, Y., Niu, C. & Cui, J. Gamma-delta (γδ) T cells: friend or foe in cancer development?
563 *Journal of Translational Medicine* **16**, 3 (2018).
564 31. Hu, G. *et al.* An IL6-Adenosine Positive Feedback Loop between CD73+ γδTregs and CAFs
565 Promotes Tumor Progression in Human Breast Cancer. *Cancer Immunol Res* **8**, 1273–1286
566 (2020).
567 32. Browning, L., Patel, M. R., Horvath, E. B., Tawara, K. & Jorcyk, C. L. <no title>. (2018).
568 33. Gentles, A. J. *et al.* The prognostic landscape of genes and infiltrating immune cells across
569 human cancers. *Nat Med* **21**, 938–945 (2015).
570 34. Foord, E., Arruda, L. C. M., Gaballa, A., Klynning, C. & Uhlin, M. Characterization of ascites-
571 and tumor-infiltrating γδ T cells reveals distinct repertoires and a beneficial role in ovarian
572 cancer. *Sci Transl Med* **13**, eabb0192 (2021).
573 35. Wu, Y. *et al.* An innate-like Vδ1+ γδ T cell compartment in the human breast is associated
574 with remission in triple-negative breast cancer. *Sci Transl Med* **11**, eaax9364 (2019).
575 36. Yuan, A., Chen, J. J. W., Yao, P.-L. & Yang, P.-C. The role of interleukin-8 in cancer cells and
576 microenvironment interaction. *Front Biosci* **10**, 853–865 (2005).

577 37. De Larco, J. E. *et al.* A potential role for interleukin-8 in the metastatic phenotype of breast
578 carcinoma cells. *Am J Pathol* **158**, 639–646 (2001).
579 38. Wen, J. *et al.* IL-8 promotes cell migration through regulating EMT by activating the Wnt/β-
580 catenin pathway in ovarian cancer. *J Cell Mol Med* **24**, 1588–1598 (2020).
581 39. Interleukin-8 promotes human ovarian cancer cell migration by epithelial-mesenchymal
582 transition induction in vitro - PubMed. https://pubmed-ncbi-nlm-nih-
583 gov.proxy.insermbiblio.inist.fr/25373532/.
584 40. Li, Y. *et al.* Effect of targeted silencing of IL-8 on in vitro migration and invasion of SKOV3
585 ovarian cancer cells. *Oncol Lett* **13**, 567–572 (2017).
586 41. Uddin, M. M., Gaire, B. & Vancurova, I. Interleukin-8 Induces Proliferation of Ovarian
587 Cancer Cells in 3D Spheroids. *Methods Mol Biol* **2108**, 117–124 (2020).
588 42. Ji, Z. *et al.* Cancer-Associated Fibroblast-Derived Interleukin-8 Promotes Ovarian Cancer
589 Cell Stemness and Malignancy Through the Notch3-Mediated Signaling. *Front Cell Dev Biol*
590 **9**, 684505 (2021).
591 43. Zhao, Z. *et al.* Epithelial-mesenchymal transition in cancer: Role of the IL-8/IL-8R axis
592 (Review). *Oncology Letters* **13**, 4577–4584 (2017).
593 44. Abiko, K. *et al.* IFN-γ from lymphocytes induces PD-L1 expression and promotes
594 progression of ovarian cancer. *Br J Cancer* **112**, 1501–1509 (2015).
595 45. Cords, L. *et al.* Cancer-associated fibroblast classification in single-cell and spatial
596 proteomics data. *Nat Commun* **14**, 4294 (2023).
597 46. Harmon, C. *et al.* γδ T cell dichotomy with opposing cytotoxic and wound healing functions
598 in human solid tumors. *Nat Cancer* **4**, 1122–1137 (2023).
599

600 **Acknowledgements**

This work was supported by the Institute National de la Santé et de la Recherche Médicale (INSERM); Université Montpellier; the Institut Régional du Cancer de Montpellier (ICM), the SIRIC Montpellier Cancer (Grant INCa_Inserm_DGOS_12553), the Fondation ARC and the Ligue contre le Cancer. Ghita Chabab is supported by a Ph. D. studentship from the Fondation pour la Recherche Médicale and Fondation ARC. We acknowledge the Clinical Resources Center of the Montpellier Cancer Institute (CRB-ICM, n°BB-033-00059). We acknowledge the imaging facility MRI, member of the national infrastructure France-BioImaging infrastructure supported by the French National Research Agency (ANR-10-INBS-04, Investments for the future).

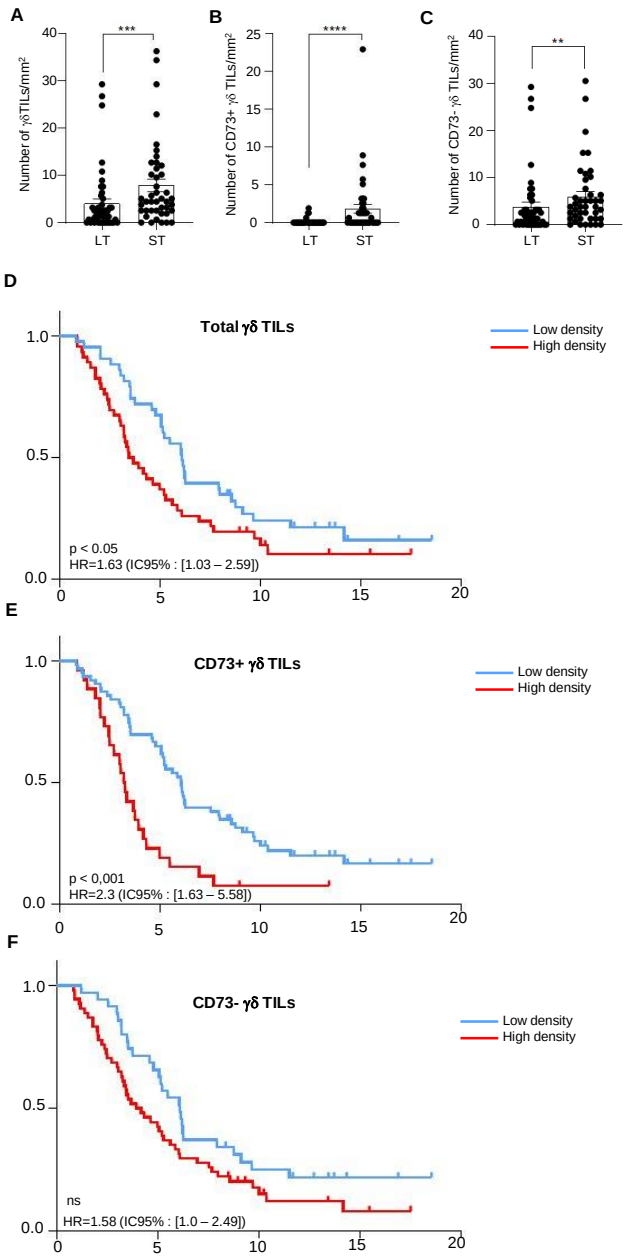

Figure 1. Impact of γδ T cells on survival of human ovarian cancer

Scatter plots comparing the density of total γδ T cells (a), CD73+ γδ T cells (b), and CD73- γδ T cells (c) in short-term (ST) to long-term (LT) survivors. Overall survival analysis according to the density of total γδ T cells (d), CD73+ γδ T cells (e), and CD73- γδ T cells (f) in the same patients with ovarian cancer. Data are the mean ± SEM. ns: not significant; **p < 0.01; ***p < 0.001; ****p < 0.0001 (Mann-Whitney test for panels a, b and c; log-rank test for the survival analysis). TILs, tumor-infiltrating lymphocytes.

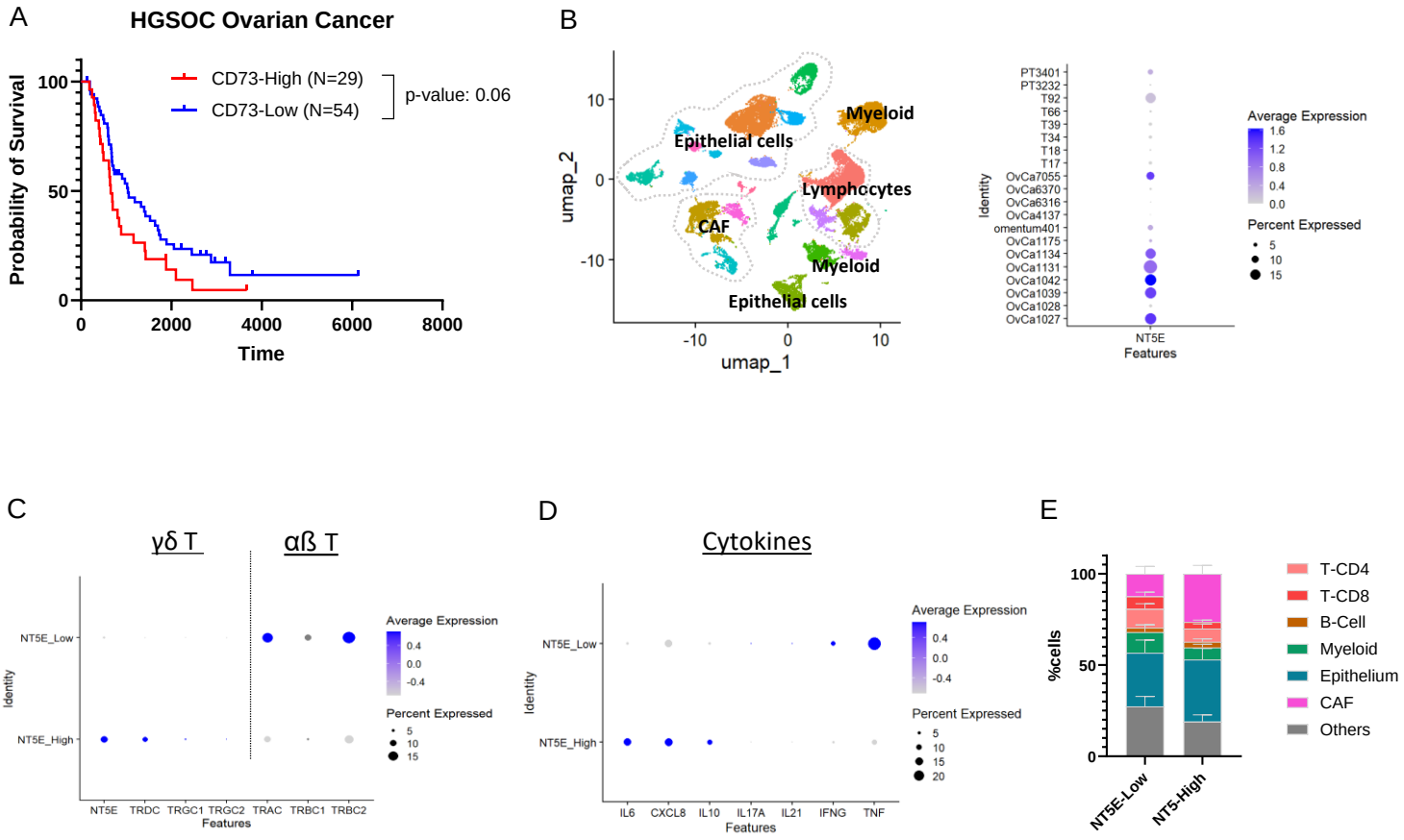

Figure2. Analysis of single-cell RNA sequencing data from 12 naive HGSOC patients

A) Kaplan-Meier survival plots comparing patient populations with low and high CD73 (NT5E) transcriptomic expression according to the TCGA dataset.

B) UMAP plot generated from single-cell RNA sequencing data of 20 naive HGSOC patients GSE147082, GSE241221 and GSE235931 datasets) showing the identification of tumor-associated cell clusters (left panel). Dot plot showing NT5E expression in the whole tumors of 20 patients (right panel).

C) Dot plot showing the expression of TCR chain genes in patients with low NT5E expression (NT5E_low, n=10) compared to high NT5E expression (NT5E_high, n= 10).

D) Dot plot illustrating cytokine gene expression in NT5E_low and NT5E_high patient groups.

E) Proportions (%) of the different cell types that compose the tumor microenvironment.

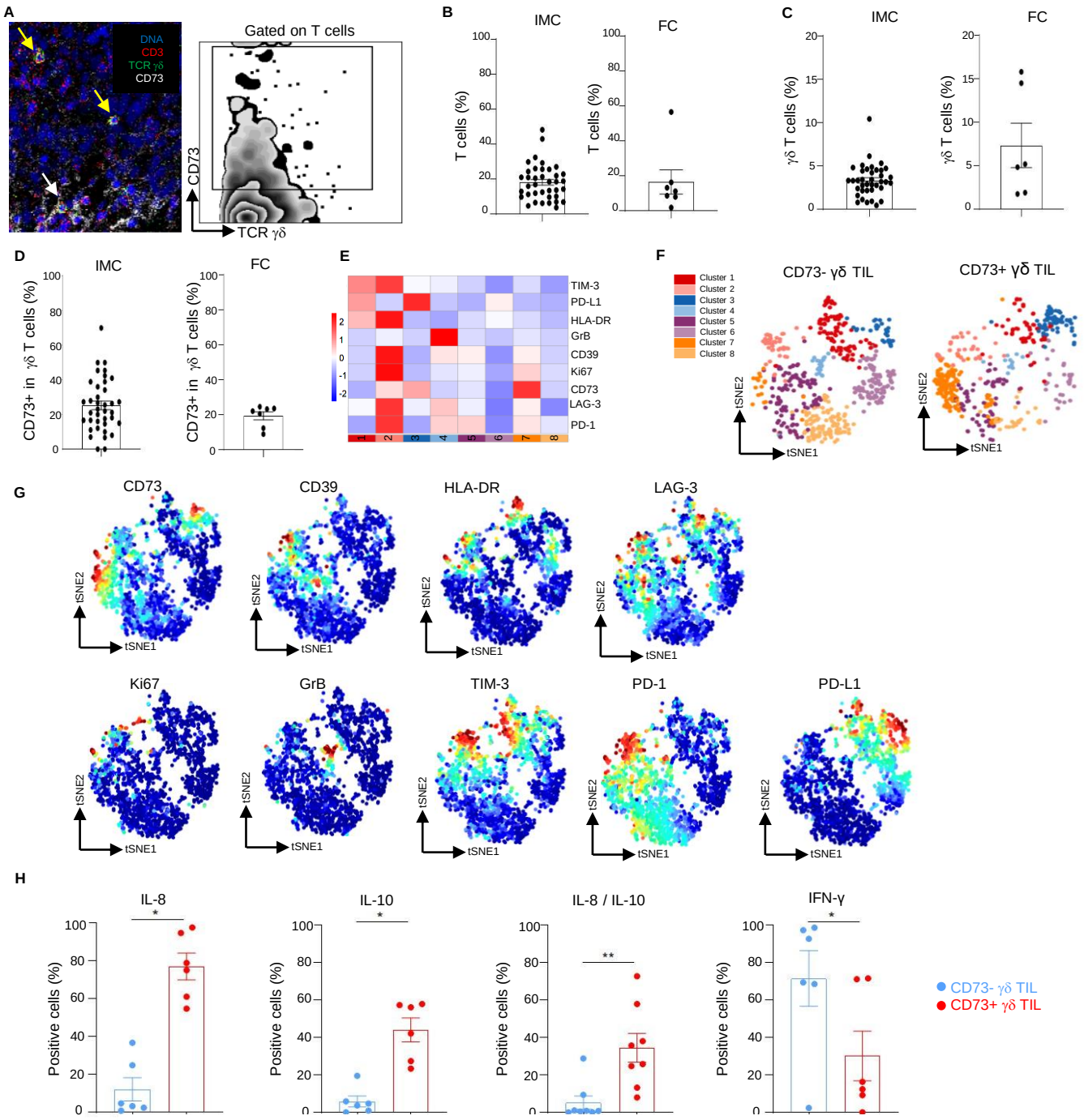

Figure 3. γδ T cell phenotype and function in ovarian cancer tissue

(A) IMC data showing CD73+ and CD73- γδ T cells in an ovarian tumor section (left panel) and the gating (right panel). Dot plots show the percentages of T cells (B), γδ T cells (C), and CD73+ γδ T cells (D) by IMC and flow cytometry (FC) analysis. For IMC plots, each black circle represents a ROI; for flow cytometry, each black circle represents a patient sample. (E) Heat map showing the clustering of γδ TILs based on the expression of the listed markers. (F) tSNE plots showing cluster repartition in CD73+ and CD73- γδ T cells. (G) tSNE plots showing the expression of each analyzed marker in the total γδ T cell clusters. (H) Dot plots showing the expression of IL-8, IL-10 and IFN-γ in CD73+ (red) and CD73- (blue) γδ TILs. Data are the mean ± SEM (n=6); **$p < 0.01$; *$p < 0.05$ (Wilcoxon signed rank test).

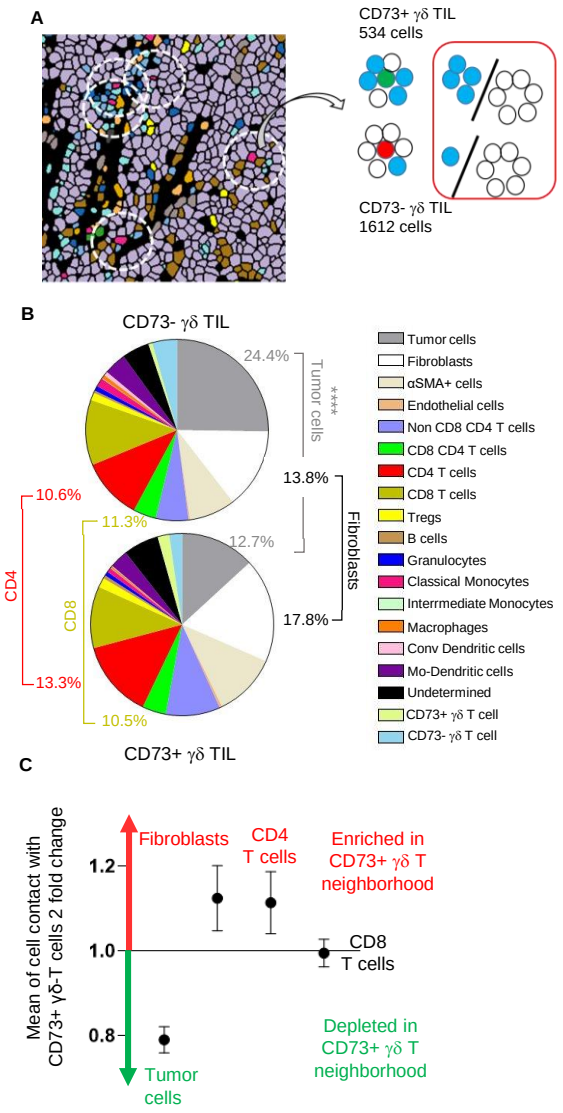

Figure 4. Neighbors of CD73+ and CD73- γδ T cells in ovarian tumor

A) IMC strategy to extract all neighbors of the CD73+ and CD73- γδ T-cell subsets. B) Pie charts showing the mean value of each identified cell type in the selected ROIs. Upper panel: Neighbors of CD73- γδ T cells; lower panel: Neighbors of CD73+ γδ T cells. ****p <0.0001 (Wilcoxon signed rank test). C) The neighborhood cell enrichment represented as the log2 fold change of cell frequency in contact with CD73+ γδ T or CD73- γδ T cells.

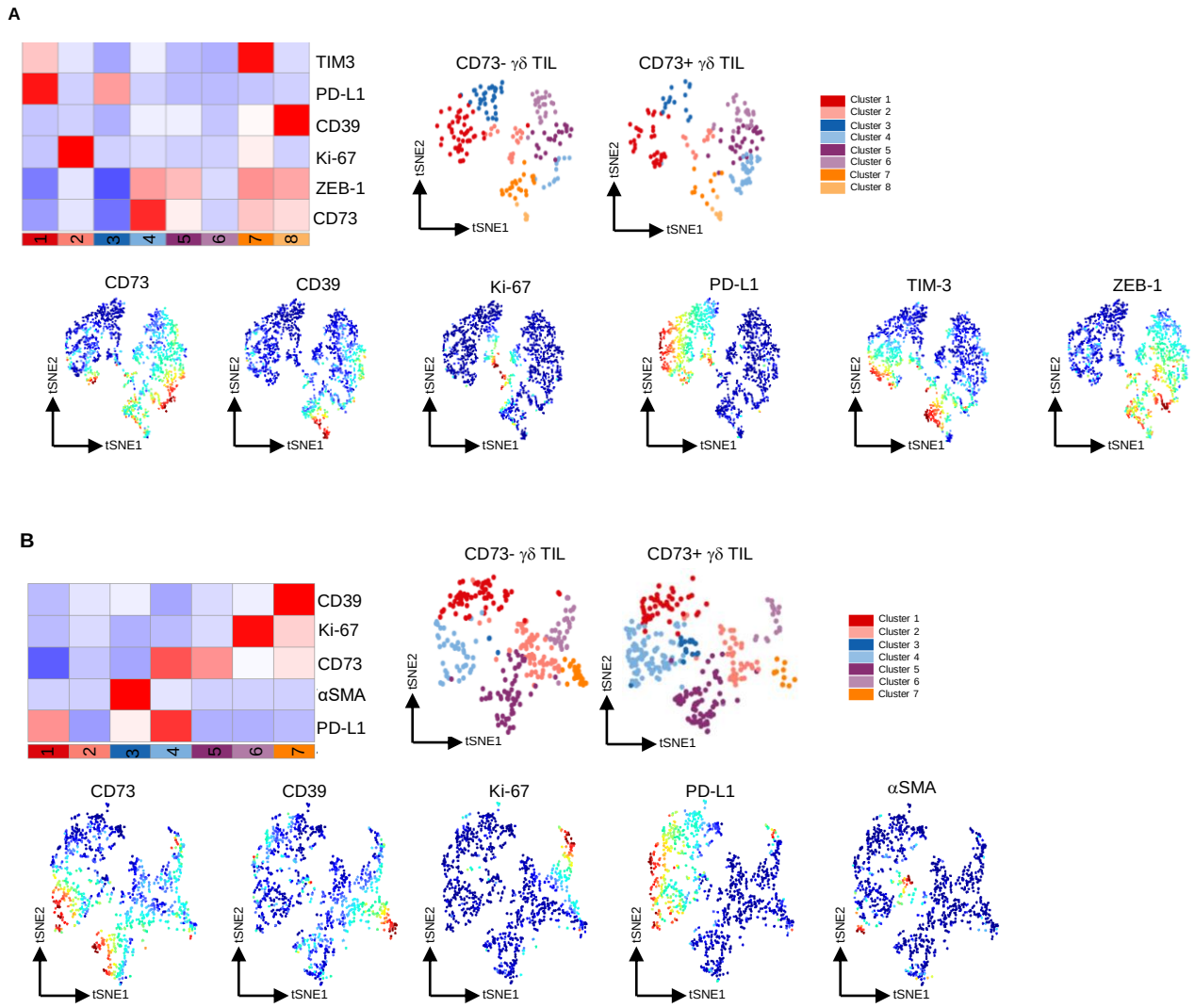

Figure 5. Phenotype of stromal neighbors of CD73+ and CD73- γδ T cell subsets

A) Heat map showing the clustering of tumor cells based on the expression of the listed markers (upper left panel) and tSNE plots showing the cluster repartition in CD73+ and CD73- γδ T cells (upper right panels). tSNE plots showing the expression of each analyzed marker in the total tumor cell clusters (lower panels). B) Heat map showing the clustering of fibroblasts based on the expression of the listed markers (upper left panel) and tSNE plots showing cluster repartition in CD73+ and CD73- γδ T cells (upper right panels). tSNE plots showing the expression of each analyzed marker in the total tumor cell clusters (lower panel).

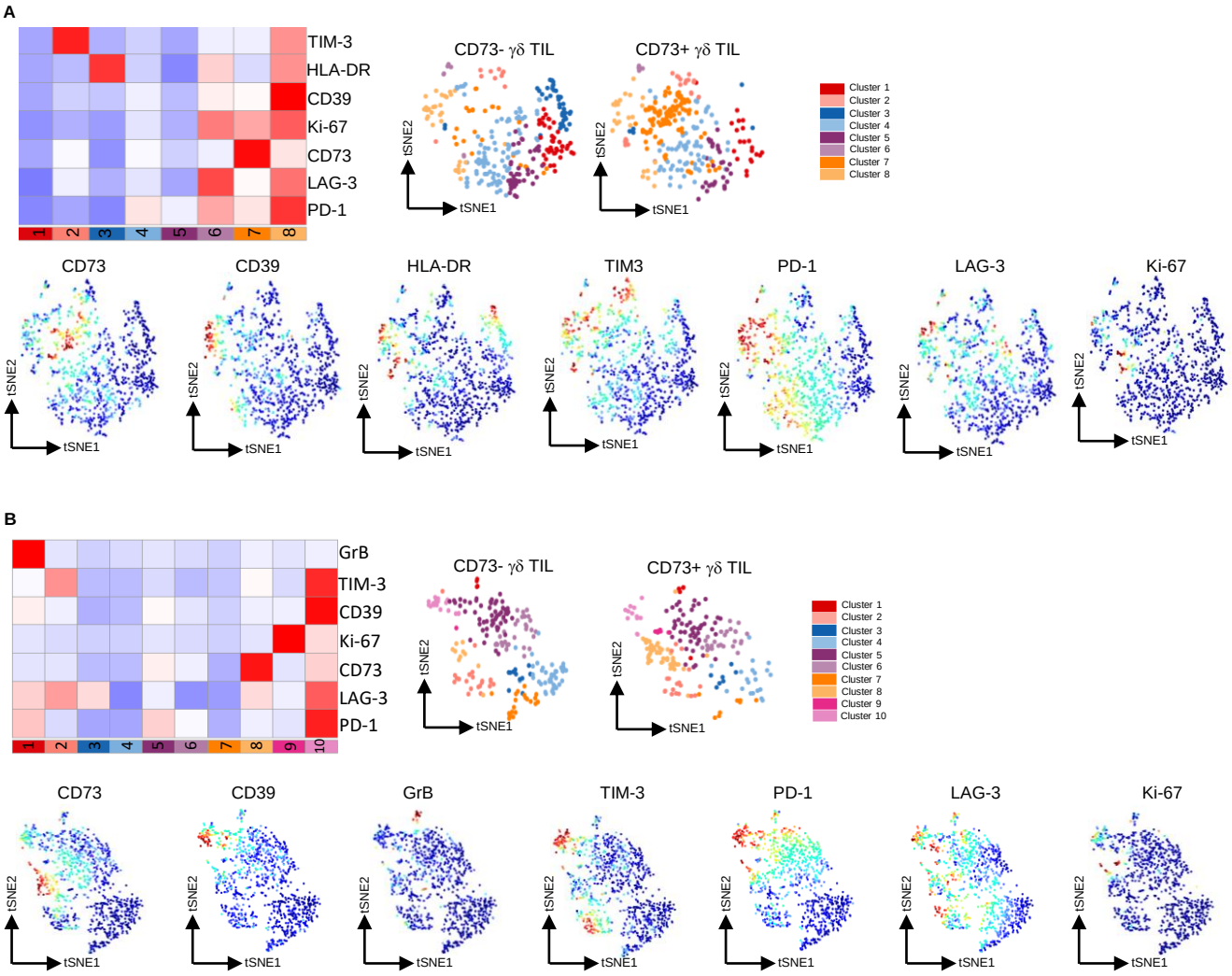

Figure 6. Phenotype of T cell neighbors of CD73+ and CD73- γδ T cell subsets

A) Heat map showing the clustering of CD4+ T cells based on the expression of the listed markers (upper left panel) and tSNE plots showing cluster repartition in CD73+ and CD73- γδ T cells (upper right panels). tSNE plots showing the expression of each analyzed marker in the total tumor cell clusters (lower panels). B) Heat map showing the clustering of CD8+ T cells based on the expression of the listed markers (upper left panel) and tSNE plots showing cluster repartition in CD73+ and CD73- γδ T cells (upper right panels). tSNE plots showing the expression of each analyzed marker in the total tumor cell clusters (lower panels).

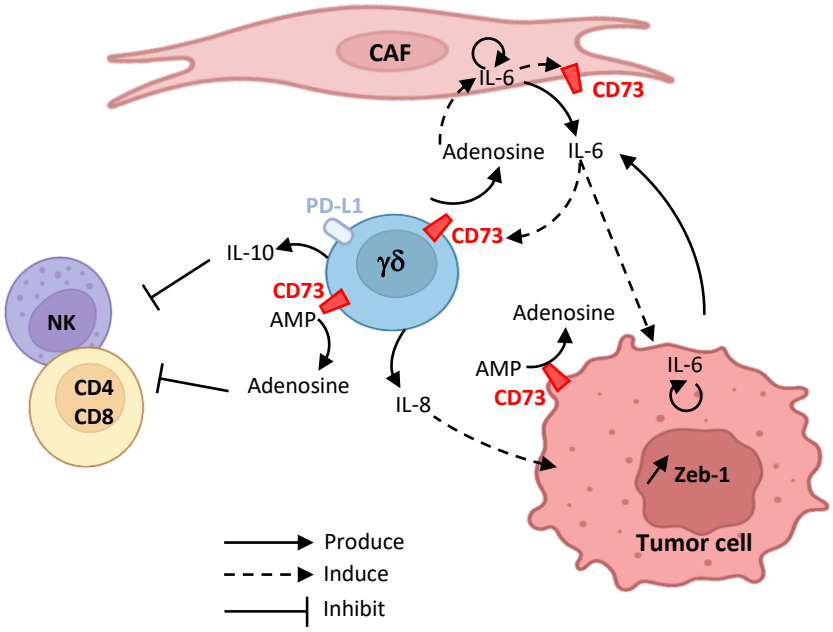

Figure 7: Schematic description of immunosuppressive mechanisms in the neighborhood of CD73+ γδ T cells

Parameter	Long-term survivors (n=48)	Short-term survivors (n=43)	Total (n=91)	p-value
Median age at diagnosis (range)	62 (22-78)	63 (33-76)	62 (22-78)	0.51 (Mann-Whitney)
Neoadjuvant treatment*				
Yes	8	6	14	0.72 (Chi2)
No	40	37	77	
FIGO stage				
III	42	37	79	0.84 (Chi2)
IV	6	6	12	
Location				
Peritoneum	13	12	25	0.32 (Fisher)
Ovary	34	27	61	
Other	1	4	5	
Lymph node invasion				
N-	12	8	20	0.37 (Chi2)
N+	32	34	66	
Missing	4	1	5	

*all samples used in this study were from biospies at diagnosis and are, thus, chemonaïve

Table S1. Clinicopathological characteristics of ovarian cancer cohort

A

Target	Clone	Supplier
CD45	HI30	BD Biosciences
CD3	SK7	BD Biosciences
GD	IMMU510	Beckman Coulter
CD73	AD2	BD Biosciences
CD39	TU66	BD Biosciences
PD1	EH12.1	BD Biosciences
PD-L1	MIH1	BD Biosciences
PD-L2	MIH18	BD Biosciences
TIGIT	741182	BD Biosciences
TIM3	7D3	BD Biosciences
Viability dye	-	Beckman Coulter

B

Target	Clone	Supplier
CD45	HI30	BD Biosciences
CD3	SK7	BD Biosciences
GD	IMMU510	Beckman Coulter
CD73	AD2	BD Biosciences
IL10	JES3-9D7	BD Biosciences
IL8	G265-8	BD Biosciences
IFN-γ	B27	BD Biosciences
Viability dye	-	Beckman Coulter

Table S2. Antibodies used for flow cytometry experiments.
Antibodies used for phenotyping are listed in table A. Antibodies used for cytokine measurment are listed in table B.

Target	Clone	Supplier	Tag
Pan CK	AE1/AE3	SantaCruz	148 Nd
Ecadherin	24E10	StandardBiotools	158 Gd
Alpha-SMA	1A4	StandardBiotools	141 Pr
Vimentin	D21H3	StandardBiotools	143 Nd
CD31	EPR3094	StandardBiotools	151 Eu
Zeb1/2	2A8A6	Novus	170 Er
CD45	D9M8I	CellSignaling tech	89Y
CD20	EP459Y	Abcam	142 Nd
CD3	D7A6E	CellSignaling tech	152Sm
CD4	EPR6855	StandardBiotools	156 Gd
Gamma Delta	H-41	CellSignaling tech	161 Dy
CD8a	C8/144B	StandardBiotools	162 Dy
FoxP3	263A/E7	StandardBiotools	155 Gd
CD14	EPR3653	StandardBiotools	144 Nd
CD16	EPR16784	StandardBiotools	146 Nd
CD11b	EPR1344	StandardBiotools	149 Sm
CD11c	EP1347Y	Abcam	154 Sm
CD68	KP1	StandardBiotools	159 Tb
CD66b	REA306	Miltenyi	153 Eu
CD15	MMA	Abcam	163 Dy
CD163	EDHu-1	StandardBiotools	147 Sm
CD208	REA295	Miltenyi	160 Gd
CD57	NK1	Abcam	145 Nd
HLA-DR	TAL-1B5	Abcam	174 Yb
Granzyme-B	EPR20129-217	StandardBiotools	167 Er
Ki-67	B56	StandardBiotools	168 Er
CD73	D7F9A	CellSignaling tech	166 Er
CD39	EPR20627	Abcam	176 Yb
Lag3	D2G4O	CellSignaling tech	164 Dy
PD-1	EH33	CellSignaling tech	165 Ho
CD366/TIM-3	D5D5R	CellSignaling tech	171 Er
PD-L1	SP142	Abcam	Uncoupled
aRb	Polyclonal	StandardBiotools	175 Lu

Table S3. Antibodies used for imaging mass cytometry